energies

MDPI

Article

Efficient Simulation of Sandbody Architecture Using Probability Simulation—A Case Study in Cretaceous Condensate Gas Reservoir in Yakela Area, Tahe Oilfield, China

Shuyang Chen [1,2], Lin Pan [1,*], Xiao Wang [1], Honggang Liang [2] and Tian Dong [1]

[1] School of Earth Resources, China University of Geosciences, Wuhan 430074, China
[2] Sinopec Northwest Oilfield Company, Urumqi 830011, China
* Correspondence: panlin@cug.edu.cn

Abstract: The Cretaceous condensate gas reservoir in Yakela is in a fan delta system in which the river channel swings frequently and the contact relationships between sandbodies are complicated both vertically and horizontally. Therefore, making the sandbody architecture clear is becoming the most urgent demand in locating the remaining oil. However, conventional well correlations and fine interpretation do not apply in this area due to the large-spacing of wells and the lack of reliable seismic data. In this paper, we analyzed the vertical characteristics of sandbody architecture including the type and thickness of architectural elements and their contact relationships based on well data, then simulated the lateral and planar distribution probabilities via a database containing a large number of dimension parameters from relevant architectural elements using Monte Carlo simulation. This simulation provides reasonable and efficient estimation of inter-well sandbody distribution. The workflow and data we present can be applied to similar clastic reservoir modeling and simulations, especially for areas with insufficient well and seismic data.

Keywords: sandbody architecture; Monte Carlo simulation; reservoir description; Cretaceous; Tahe Oilfield

Citation: Chen, S.; Pan, L.; Wang, X.; Liang, H.; Dong, T. Efficient Simulation of Sandbody Architecture Using Probability Simulation—A Case Study in Cretaceous Condensate Gas Reservoir in Yakela Area, Tahe Oilfield, China. *Energies* **2022**, *15*, 5971. https://doi.org/10.3390/en15165971

Academic Editor: Ernst Huenges

Received: 16 July 2022
Accepted: 16 August 2022
Published: 18 August 2022

1. Introduction

Sandbody architecture (also known as reservoir architecture, sandbody geometry, or reservoir heterogeneity) analysis is one essential method for clastic reservoir modeling, especially in the late stage of oil/gas field development, to locate the remaining oil/gas [1–9]. Sandbody architecture research originated from outcrop anatomies and aimed to provide data on the background sedimentary facies, environments, and evolutions of a specific reservoir [10–12]. With the development of subsurface techniques such as well logging, seismic, radar, and lidar, integrated with outcrop achievements, researchers have been marching towards realistic reconstructions of genetic stratigraphy and reservoir architecture in costal/shelf and fluvial reservoirs, specifically in meandering river systems [13–22]. Meanwhile, in fan delta reservoirs, the sediment commonly consists of a high proportion of coarse material that is seasonally transported through a series of distributary channels of braided river, and thus is more complicated in sandbody distribution and connection compared to marine reservoirs or fluvial systems [10]. As a result, deltaic reservoirs had not been examined in the aspect of architecture as thoroughly as shelf reservoirs or meandering river channels until recent years [23–25].

From previous research we can conclude the prerequisites of reservoir architecture analysis are finely described outcrops, closely spaced wells, or seismic data with high resolution and accuracy. Thus, it is challenging to carry out the fine characterization of reservoir architecture in areas of widely spaced wells with no reliable seismic data.

The Yakela Cretaceous condensate gas reservoir (YKL), which has been producing stably for over 20 years, is the largest self-contained condensate gas reservoir of Sinopec and one of the sources of gas transportation from the west to the east in China [26]. With the deepening of fine development, it is urgent to make the distribution characteristics of the reservoir clear. Unfortunately, in this area the well spacing is large (the average distance is ~1500 m compared to 150~300 m in a fluvial reservoir), and the seismic data is of poor quality due to the harsh operating environment (high latitude Gobi Desert) and complicated subsurface structure (multiple severe tectonic movements in buried history). Under these conditions, it is exceedingly difficult to estimate the reservoir architecture and obtain a reliable reservoir model.

Here we present a feasible and reasonable workflow for reservoir architecture estimation under the circumstance of lacking well and seismic data. According to Walther's Law of facies, which states that the vertical succession of continuous sedimentary facies reflects lateral changes in their environment [27,28], it is possible to estimate the lateral developments from the limited data of vertical characteristics through reasonable simulation. We first summarize the vertical distribution probabilities of the target reservoir based on cores, well logs, and test data, and then carry out a Monte Carlo simulation using the vertical distribution probability through a training model of reservoir architectural elements to estimate the spatial distribution probability of the reservoir elements in the study area. The simulation's result is validated by the later seismic-interpretated reservoir model. This efficient simulation can be further applied to similar fan delta reservoirs to improve or validate the accuracy of reservoir modeling.

2. Geological Background

The Tarim Basin in northwestern China covering an area of 560,000 km^2 and is the largest petroliferous basin in China. This basin can be divided into seven structural zones, including the Kuqa depression, the Taibei Uplift Belt, the Northern Depression Belt, the Central Uplift Belt, the Southwestern Depression Belt, the Southeastern Uplift Belt, and the Southeastern Depression Belt [29–32]. The Yakela gas reservoir is in the Yakela sag in the Taibei Uplift Belt (Figure 1).

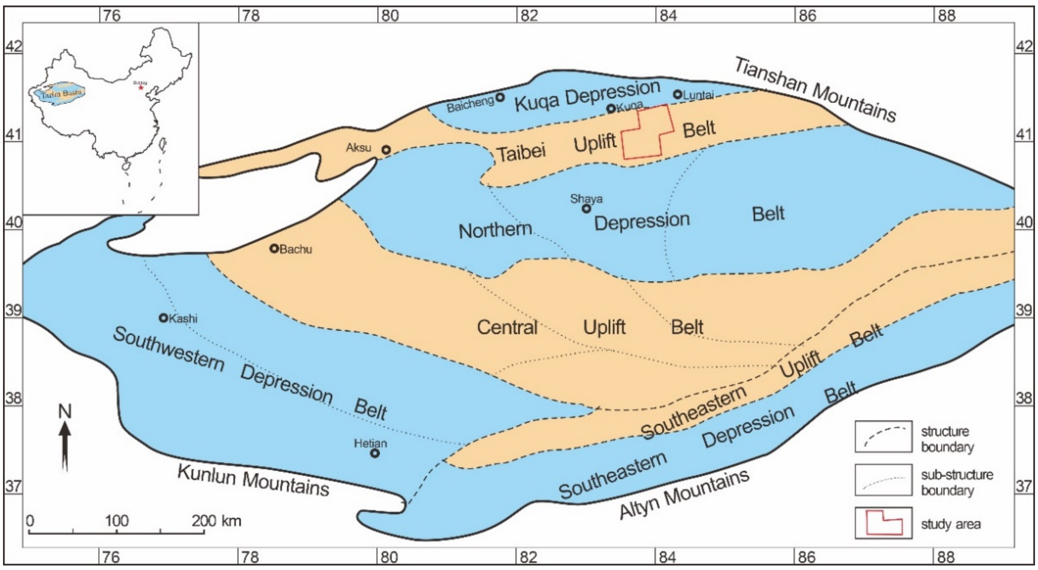

Figure 1. Structural map of Tarim Basin and the location of the study area.

The strata revealed in the study area include (from bottom to top) Proterozoic, Upper Cambrian, Lower Ordovician, Upper Devonian, Lower Carboniferous, Upper Triassic, Lower Jurassic, Lower Cretaceous, Paleogene, Neogene, and Quaternary (Figure 2). The target layer of this research is the clastic reservoir in the Cretaceous Yageliemu Formation (K_1y).

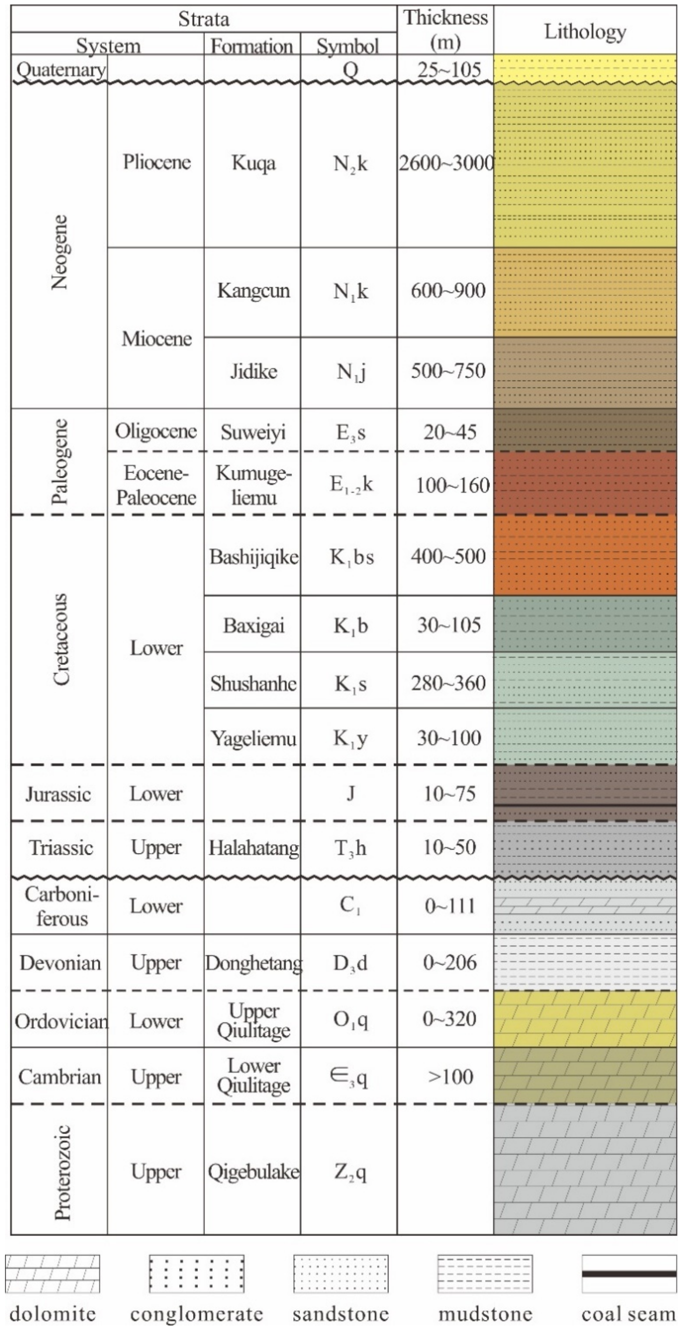

Figure 2. Stratigraphy column of study area.

The K_1y condensate gas reservoir has a gas-bearing area of 38.6 km^2. It is a normal temperature and pressure system with deep burial depth (>5300 m), no oil ring, medium condensate content (~234 g/m^3), a large water body (~100 times), low porosity (10–15%), and medium-to-low permeability (10–150 mD). There are, in total, 43 wells in this area, with a minimum well spacing of 234 m and an average well spacing of ~1500 m. This well spacing is quite large compared to the average value of 100~200 m in previous sandbody architecture research. Regional sedimentary facies studies suggest that the K_1y reservoir can be divided into the lower transgressive lake fan delta and the upper regressive braided river delta sedimentary systems, and that the microfacies include braided distributary channels, distributary channels, flood plains, inter-distributary bay, and sand bars [6,33].

3. Methodology

The overall methodology is first summarizing the vertical distribution probability of reservoir architectural elements as a testing dataset, then building a reservoir architectural element database as a training dataset for a Monte Carlo simulation, and finally, applying the testing dataset in the simulation model to get the horizontal distribution probability of the reservoir (Figure 3).

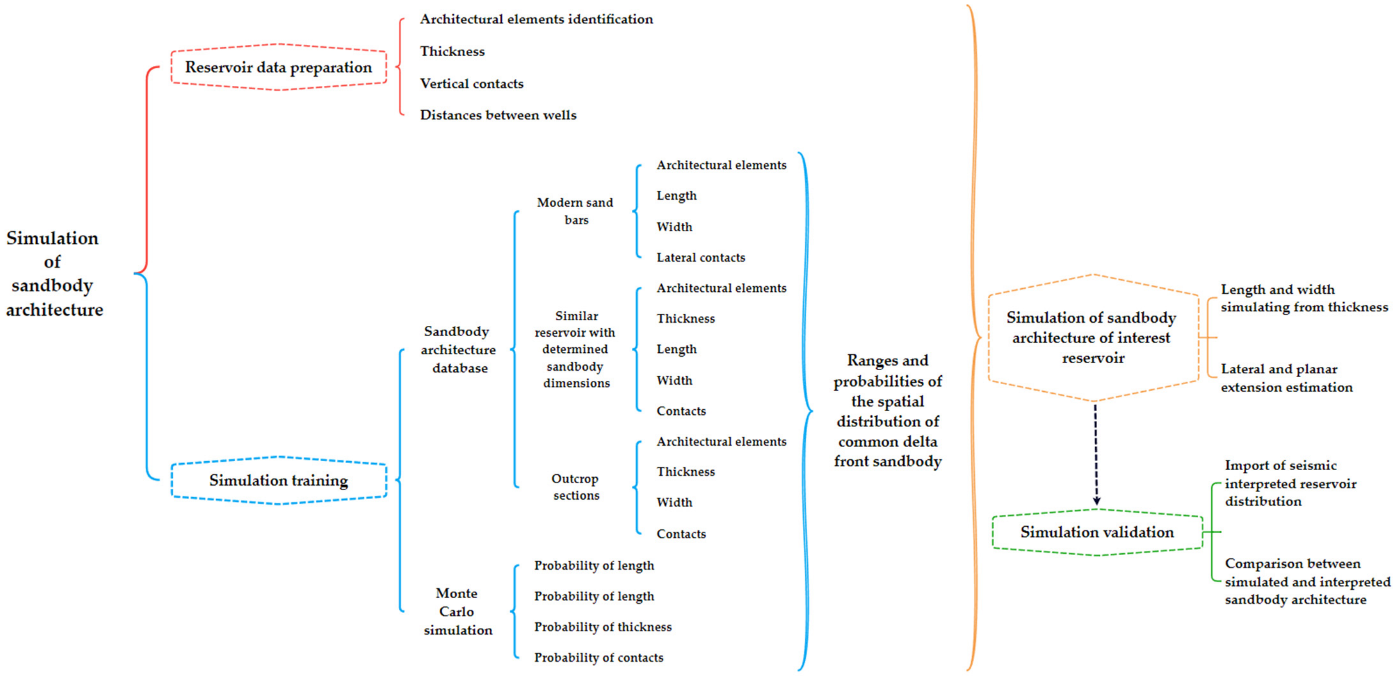

Figure 3. Systematic workflow.

3.1. Reservoir Data Preparation

Well data of study area include core measurements of porosity and permeability (138 data sets), core observations (23 wells, 253 m in total), and well logs (SP, GR, AC, DEN, R, CNL for 39 wells). We used these data to analyze the microfacies and determine the parameters of architectural elements, including thickness, vertical contact relationships, and horizontal distances between wells. The vertical architectural element parameters then served as the testing dataset for the probability estimation of sandbody development and distribution.

3.2. Building Sandbody Architectural Element Database

As the well data primarily reveal vertical distribution characteristics, we introduced multiple analogue data to build a sandstone architecture database containing the length, width, and thickness of sandbodies. This database served as training dataset on sandbody development and distribution probability. The analogue data include measured dimensions of modern sand bars, similar reservoirs, and outcrop sections.

3.2.1. Modern Sand Bars

We observed and measured the satellite images of the Yangtze River Delta in the Google Earth satellite map (Figure 4), then analyzed the planar geometric and morphological characteristics of the sandbars at the Yangtze River mouth. The channel at the estuary of the Yangtze River Delta has a large amount of sediment of significant width, indicating a fast sediment-deposition rate. The estuary sandbars are formed primarily by sedimentation and river erosion, with few disturbances by human activities. According to the results of measurement and statistics, the sandbars can be categorized into four shapes (Figure 5): (1) Elongated, the sandbar is strip-shaped (the ratio of length to width greater than 3), and the rear of the sandbar is flat; (2) Oval, the two ends of the sandbar are approximately arc-shaped, and the whole body looks like an oval shape; (3) Elongated cone, one end of the sand dam is flat, and the other one is of a triangle shape. The length to width ratio of the sand dam is greater than 3; (4) Special shapes, some of the sandbars are more complex in shape and can be categorized to special shapes. The measurement results of the shape, area, length, and width of each sandbar show that oval is the common shape of the sandbars, the length of the sandbars ranges in 400–600 m, and the width is mainly distributed 50–300 m (Table 1).

Figure 4. Location of modern sandbars for distant measurement.

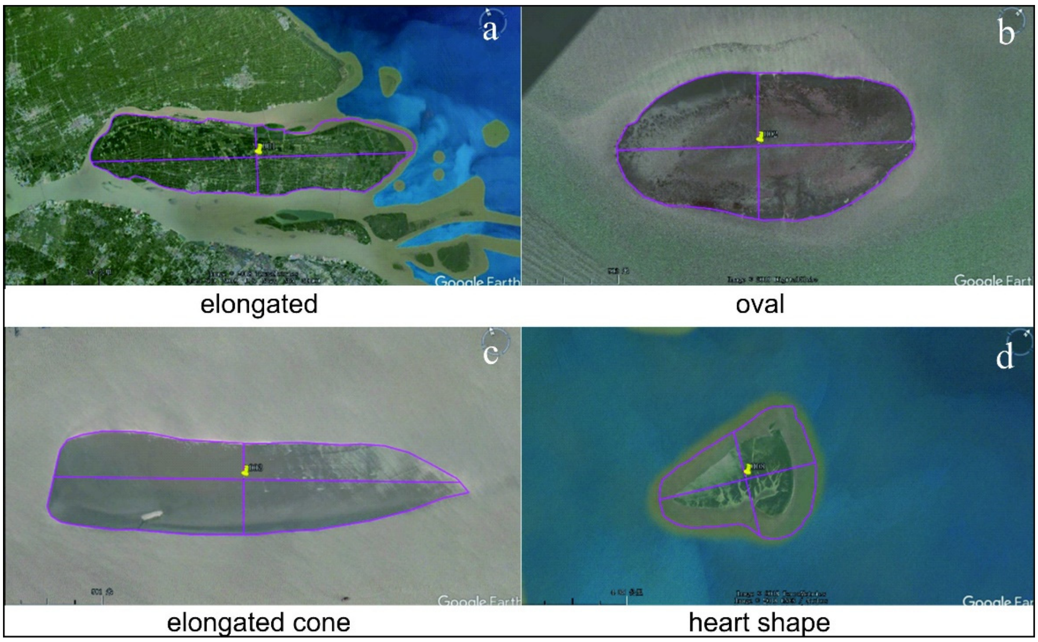

Figure 5. Examples of the shape and measuremnt of morden sandbars.

Table 1. Detailed measurements of modern sandbars.

No.	Shape	Length (m)	Width (m)
01	oval	1364	676
02	elongated	1879	415
03	Special shape: quadrilateral	249	198
04	Special shape: fan shape	785	510
05	oval	197	95
06	oval	836	433
07	Special shape: irregular	500	177
08	Special shape: fan shape	433	246
09	Special shape: quadrilateral	430	240
010	oval	1078	370
011	elongated cone	873	523
012	Special shape: quadrilateral	556	533
013	elongated cone	489	269
014	elongated cone	483	198
015	oval	80	24
016	Special shape: leaf shape	86	21.4
017	oval	231	55
018	elongated	151	22
019	elongated cone	741	276
020	elongated cone	438	250
021	elongated	976	309
022	elongated cone	453	229
023	elongated cone	471	224
024	elongated cone	492	269
025	elongated cone	435	168

3.2.2. Similar Reservoir—Triassic Fluvial Reservoir of Block 1 in Tahe Oilfield

The stratigraphic structure and lithological properties of the K_1y reservoir are similar to the braided river delta deposition of the Lower Triassic reservoir of Block 1 in Tahe Oilfield. The Lower Triassic reservoir in Block 1 uses fine seismic interpretation and well logs to discriminate the sandbody boundary. The sandbars in Block 1 are mainly spindle-shaped, with lengths ranging from 200–500 m and widths ranging from 200–400 m (Table 2).

Table 2. Interpreted dimensions of sandbars in Block 1.

No.	Shape	Length (m)	Width (m)	Thickness (m)
1	elongated cone	672	321	8.1
2	elongated cone	516	263	7.44
3	elongated cone	381	230	4.86
4	elongated cone	423	209	5.56
5	elongated cone	500	272	7.15
6	elongated cone	429	231	6.8
7	elongated cone	428	207	8.86
8	elongated cone	428	209	5.92
9	elongated cone	536	330	7.92
10	elongated cone	731	361	8.7
11	elongated cone	611	269	8.38
12	elongated cone	780	307	10.42
13	elongated cone	540	254	8.32
14	elongated cone	492.75	238.5	5.28
15	elongated cone	425	329	9.5

Table 2. *Cont.*

No.	Shape	Length (m)	Width (m)	Thickness (m)
16	elongated cone	565	287	5.06
17	elongated cone	465	267	8.22
18	elongated cone	517	258	6.2
19	elongated cone	503	315	8.22
20	elongated cone	482	252	4.96
21	elongated cone	427	248	8.52
22	elongated cone	329	212	7.44
23	elongated cone	780	407	10.42
24	elongated cone	540	354	8.32
25	elongated cone	659	392	9.28
26	elongated cone	515	396	10.96
27	elongated cone	641	459	12.18
28	elongated cone	662	297	10.34
29	elongated cone	578	383	11.05
30	elongated cone	499	343	10.06
31	elongated cone	573	357	10.92
32	elongated cone	694	421	13.32

3.2.3. Outcrop Sections

We employ a set of sandstone architecture parameters based on field measurements of the Jurassic delta front outcrops in Yichang (central China), which had a complete exposure due to construction digging and thus can be tracked horizontally and vertically (Figure 6). The thickness of the sandbar of the delta front ranges from 1.5–2.1 m with an average value of 1.7 m, the width 11–22 m averaged at 17 m, and the width-to-thickness ratio is 7.5–12, averaged at 9.6 (Table 3). In addition, we summarized outcrop measurements from previous published articles to have more references for the lateral development characteristics of sandbodies.

Figure 6. Jurassic delta outcrop in Yichang.

Table 3. Measurements of Jurassic delta from outcrop sections in Yichang.

Sandbody Type	Shape	Width (m)	Thickness (m)
River mouth bar	convex lenticular (both top and bottom surfaces)	11.2	1.5
		18.2	2.1
		16.9	1.4
		22.4	2.1
		16.8	1.82
Subaqueous distributary channel	concave lenticular (bottom surface)	7.6	1.4
		22.4	2.8
		16.1	2.1
		7	0.9
		8	1.2
		19	2
		23	4.5
distributary channel	Top surface flat, bottom surface convex	110	1.5
		82	3.7
		155	3
		115	5.8
		89	4
		88	3.3

3.3. Monte-Carlo Simulation

In this study, we used the Monte Carlo method to simulate the probability distributions of the reservoir dimensions and the contacting relationships based on Walther's Law, i.e., the lateral extension and connection of sandbodies can be estimated through the vertical development characteristics. Monte Carlo simulations are used to model the probability of different outcomes in a process that cannot easily be predicted due to the intervention of random variables. It is also referred to as a multiple probability simulation. The essential idea of the Monte Carlo method is using randomness to solve problems that might be deterministic in principle [34]. The basis of a Monte Carlo simulation is that the probability of varying outcomes cannot be determined because of random variable interference. Therefore, a Monte Carlo simulation focuses on constantly repeating random samples to achieve certain results.

A Monte Carlo simulation takes the variable that has uncertainty and assigns it a random value. The model then runs, and a result is provided. This process is repeated again and again while assigning the variable in question many different values. Once the simulation is complete, the results are averaged together to provide an estimate. This method has been used in reservoir engineering calculations such as oil reserve estimation [35–37], and we believe more applications of the Monte Carlo simulation can be made as big data technology develops. The Monte Carlo simulation program we use is the embedded program in MATLAB. The data settings can be seen in Table 4. We carried out testing runs using the thickness data of Block 1 to simulate the length and width, and the result matched 86.25% of the original ones, suggesting this simulation has a good fit and can be employed to estimate the spatial extensions of YKL sandbodies.

Table 4. Settings of the Monte Carlo simulation.

Parameters		Setting
Input	Thickness, contact code of YKL sandbodies	Original frequency distribution from well data
	Length and width of modern sandbar Length, width, and thickness of analogue reservoir Block 1 Thickness and width of outcrops	Statistics from real data and forms the relationships of the three dimensions of sandbodies
Output	Length and width of YKL sandbodies	
Number of runs		1×10^6

4. Results

4.1. Architectural Elements Identification in Wells

As in previous research, the architectural elements developed in K_1y of the study area include distributary channel, channel side, sandbar, interdistributary bay in delta plain, and subaqueous distributary channel, subaqueous channel side, subaqueous sandbar, and subaqueous interdistributary bay in subaqueous delta front, among which the subaqueous distributary channel is the most common element. Our work in this study was to establish the well logs interpretation from the lithofacies observed from cores (Table 5) and apply them to identify these architectural elements in each well. An example of architectural element determination can be seen in Figure 7.

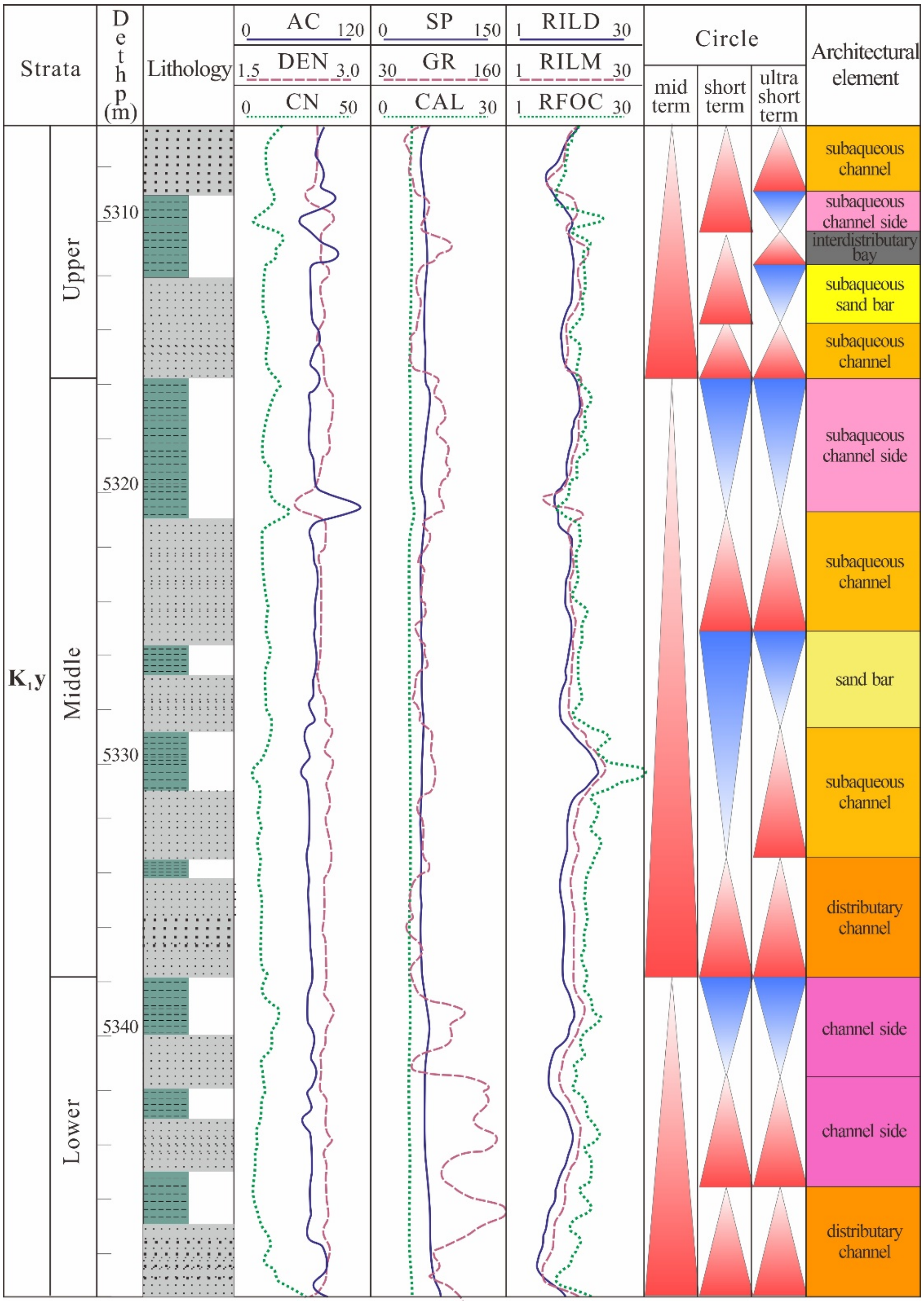

Figure 7. Bounding surfaces' discrimination and sandstone architectural element determination of a typical well in Yakela area.

Table 5. Lithofacies and well log interpretations of architectural elements.

Architectural Element		Lithofacies	Well Log Facies	
Fan delta plain	Distributary channel	Fining upward	Low amplitude bell shaped/cylinder shaped	
	Sandbar	Coarsening upward	Funnel shaped	
	Channel side	Interlayering of sandstones and mudstones	High amplitude cylinder shaped	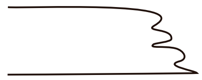
	Interdistributary bay	Mudstone predominant, containing conglomerate or thin sandstone layers	Middle-high amplitude folk shaped	
Fan delta front	Subaqueous distributary channel	Fining upward (finer than distributary channel)	Low amplitude bell shape/cylinder shaped	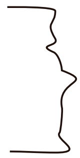
	Subaqueous sandbar	Coarsening upward (finer than distributary channel)	Funnel shaped	
	Subaqueous channel side	Thin layers, interlayers of sandstones and mudstones	Middle-high funnel shaped	
	Subaqueous interdistributary bay	Mudstone predominant, occasional sandstone seam	High amplitude fork shaped	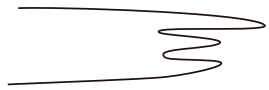

4.2. *Vertical Distributional Characteristics of Architectural Elements*

We summarized the thickness portions of each architectural element and their vertical contact relationships in all the wells. These vertical distributional characteristics then served as a testing dataset for sandbody horizontal development estimation.

4.2.1. Thickness Portions of Architectural Elements

The probability distribution of the thickness portions of each architectural element in all the wells is shown in Figure 8. For the architectural elements of the fan-shaped delta plain, the distributary channel, channel side, sandbar, and interdistributary bay account for 38%, 21%, 12%, and 29%, respectively, making their ratios Distributary channel: sandbar: channel side: interdistributary bay $\approx$ 4:2:1:3. Among the architectural elements of the front edge of the underwater fan-shaped delta, the distributary channel accounts for 42%; and the sandbar, channel side, and interdistributary bay take up 29%, 13%, and 16%, respectively. The ratio of subaqueous distributary channel: sandbar: channel side: interdistributary bay $\approx$ 4:3:1:2.

4.2.2. Vertical Contact Relationships and Their Portions

Three vertical contact (stacking) relationships of architectural elements were recognized in K_1y reservoir: continuous stacking, intermittent stacking, and erosional stacking. Continuous stacking is the smooth vertical stacking through which sandbodies form a compete rhythm without mudstone interlayers. Intermittent stacking is similar to continuous stacking but with mudstone interlayers. Channel sedimentation maintenance complete sequence, with sandstones separated by sandbodies, and erosion superposition. Erosional stacking, also known as down-cut superposition, is the downward intrusion of a late-stage channel into an early-stage channel, resulting in superimposition of different sandbodies. The erosional stacking in appearance is similar to a single sandbody, whereas it often has multi-rhythmic combinations.

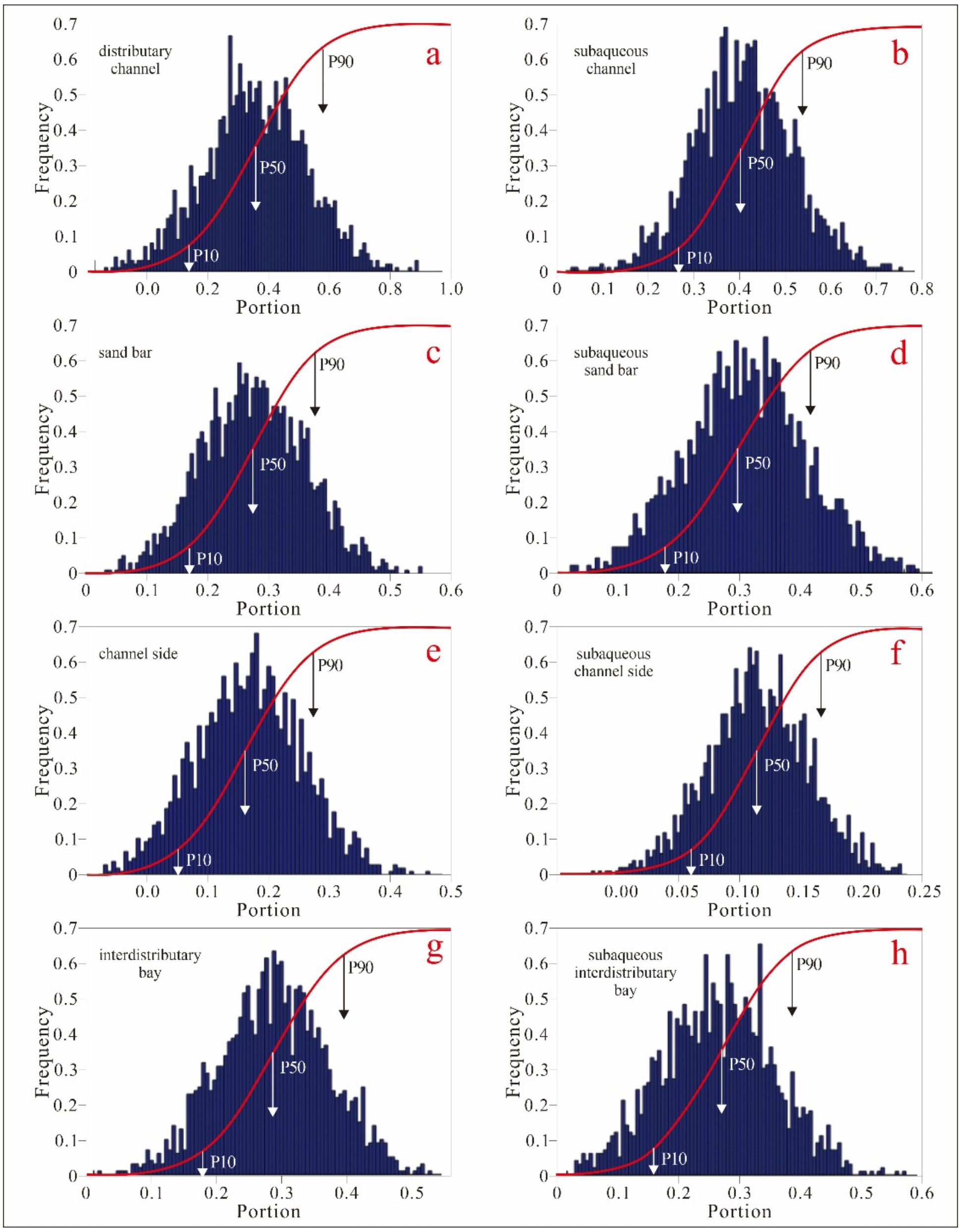

Figure 8. Probability distributions of architectural elements in all wells showing best estimate (P50), high estimate (P10), and low estimate (P90). The delta plain elements are on the left and the corresponding subaqueous delta front elments are on the right. (**a**): distributary channel; (**b**): subaqueous channel; (**c**): sand bar; (**d**): subaqueous sand bar; (**e**): channel side; (**f**): subaqueous channel side; (**g**): interdistributary bay; (**h**): subaqueous interdistributar bay.

Calculated from the probability statistics of vertical contact relationships (Table 6), the ratio of continuous stacking: erosional stacking: intermittent stacking ≈ 4.5:4.3:1.2, indicating the most common vertical contact relationship of architectural elements is continuous stacking, while the intermittent stacking is rare. Further we summarized and compared the probabilities of all possible vertical combinations of any two architectural elements (Figure 9). The results show that distributary channel–distributary channel and distributary channel–sandbar are the most-common vertical combinations in both the delta plain and the subaqueous delta front, which means above and beneath a distributary channel would probably be a distributary channel or a sandbar. This is also one important rule for lateral contact relationship estimation following Walther's Law.

Table 6. Probability statistics of vertical contact relationships of architectural elements.

Vertical Contact Relationship	Accumulative Probability		
	P10	P90	P50
Continuous stacking	0.33	0.58	0.45
Erosional stacking	0.29	0.48	0.43
Intermittent stacking	0.01	0.24	0.12

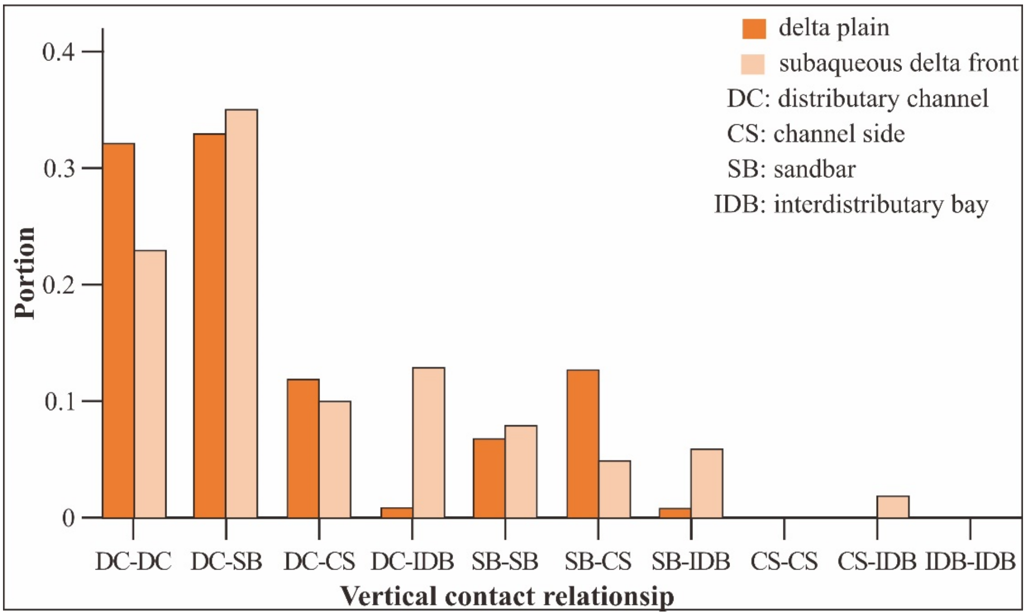

Figure 9. Vertical combinations of architectural elements and their portions.

4.3. Probability Simulation of Sandbody Dimensions

The simulated probability of the horizontal (inter-well) extension of the sandbodies using the vertical distribution of the sandbar and channel side (two major reservoir types) is shown in Figure 10. The thickness of the sandbar is mainly distributed in the range of 1–5 m. The simulated width is mainly distributed in the range of 100–300 m and the simulated length ranges of 100–500 m (Table 7). For subaqueous sandbar, the thickness primarily ranges 2–5 m, and the simulated width and length probably ranges 100–300 m and 100–500 m, respectively. The simulated shape of the sandbars is mostly oval to elongate coned. The thicknesses of both the channel side and subaqueous channel side evenly distribute in the range of 1–4 m. The simulated width is limited to the range of 100–200 m, and the simulated length ranges 100–400 m. The shapes are elongated.

Table 7. Statistics of simulation results.

Name		Count	Mean	Error	Convergence
Sandbar	Length	468,593	252	3.55	converged
	Width	586,463	391	2.56	converged
Subaqueous sandbar	Length	732,581	206	1.51	converged
	Width	696,534	352	2.64	converged
Channel side	Length	259,867	188	3.03	converged
	Width	452,898	267	2.71	converged
Subaqueous channel side	Length	554,396	145	2.89	converged
	Width	359,122	229	3.62	converged

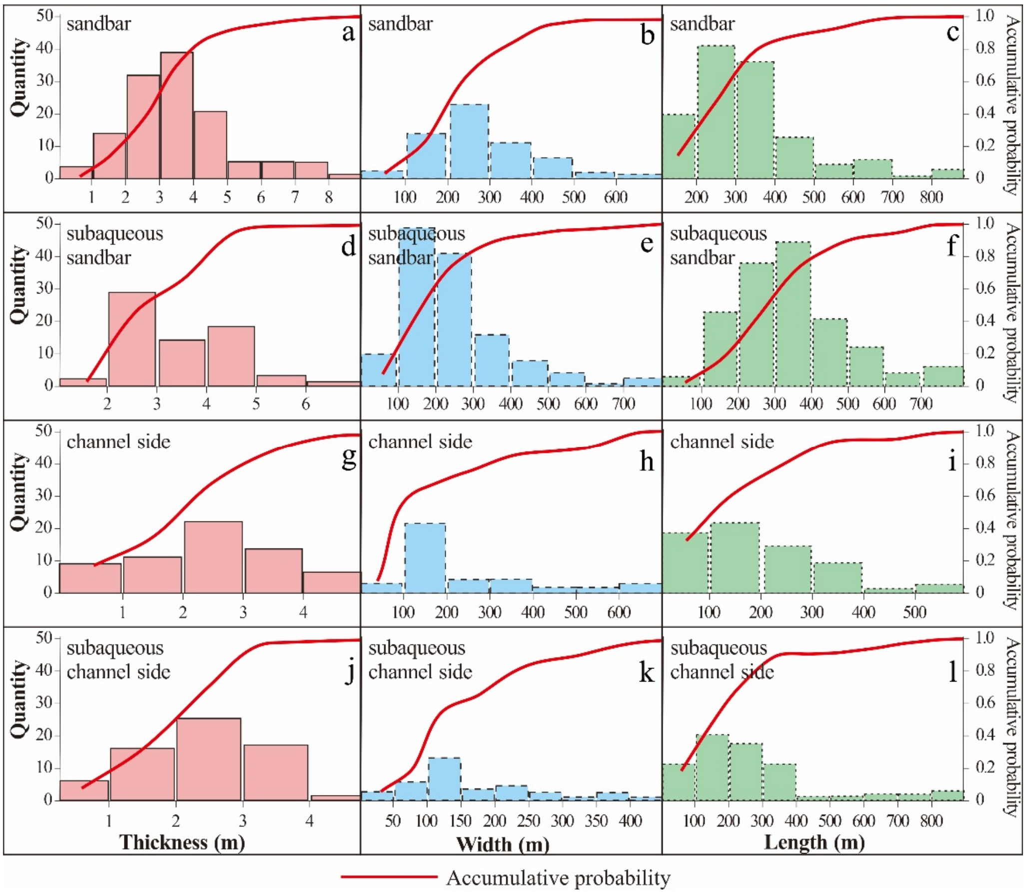

Figure 10. Thickness and simulated lateral dimension of architectural elements. The red line shows the accumulative probability. (**a**): thickness probabity of sandbar; (**b**): width probability of subaqueous sandbar; (**c**): length probability of subaqueous sandbar; (**d**): thickness probabity of subaqueous sandbar; (**e**): width probability of subaqueous sandbar; (**f**): length probability of subaqueous sandbar; (**g**): thickness probabity of channel side; (**h**): width probability of channel side; (**i**): length probability of channel side; (**j**): thickness probabity of subaqueous channel side; (**k**): width probability of subaqueous channel side; (**l**): length probability of subaqueous channel side.

4.4. Simulated Reservoir Distribution Characteristics

4.4.1. Lateral Extension

Based on the simulated dimensions of sandbodies, we connected main production wells to form skeleton well sections. Viewed from the well sections, the subaqueous distributary channel of Lower K_1y is thicker in two directions, and the range of the interdistributary bay is small. The subaqueous distributary channel and sandbar are the main elements; in Middle K_1y the lake basin continued to expand, with strip-shaped and lens-shaped sandbar deposits developed. In Upper K_1y water energy weakened but was relatively stable, so this horizon is dominated by fine-grained distributary channels, sandbars and channel sides. The distributary channel of the lower member of K_1y is thicker in the south and north than in the center, and sandbars are wide in this member. The sandbars in the middle member are narrow and shaped lenticularly on sections, and the interdistributary bay and channel side develop on both sides of distributary channel, indicating the expansion of the lake basin. In the upper member, the grain size of the subaqueous distributary channel, sandbar, and channel side are smaller than that in the middle and lower member, indicating the weakening of water energy (Figure 11). The distributary channel and sandbar are the predominant architectural elements of sandbodies, making favorable reservoir property in this area.

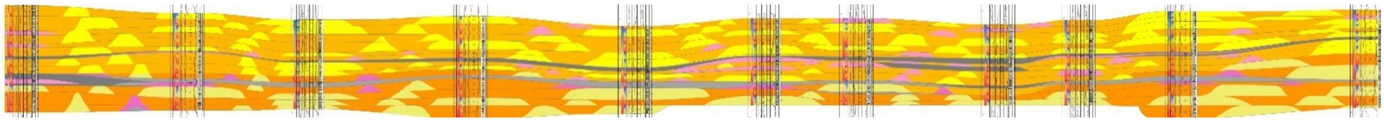

Figure 11. A typical well section showing the lateral extension of sandbodies. The location of this section is shown in Figure 11.

4.4.2. Planar Distribution

The planar distribution characteristics vary in each layer of K_1y, but the common rule is that the sandbodies have the axis of south–north (the regional depositional source direction), thus reservoir heterogeneity is strong in the west–east direction and in the eastern part the distributary channels is narrower comparing to those in the western part. Taking Layer 13 (the top layer of the lower member) for example, the subaqueous facies distribute in the southern part, where subaqueous sandbars are scattered and the subaqueous interdistributary bays are developed. In the northern part, the sandbars and channel sides are densely distributed, whereas interdistributary bay is rare (Figure 12). The area between S83 and YK9X dominantly developed subaqueous distributary channels, sandbars, channel sides, and interdistributary bays, indicating that the reservoir has good properties. Despite the producing wells, there are still good reservoirs yet to be explored.

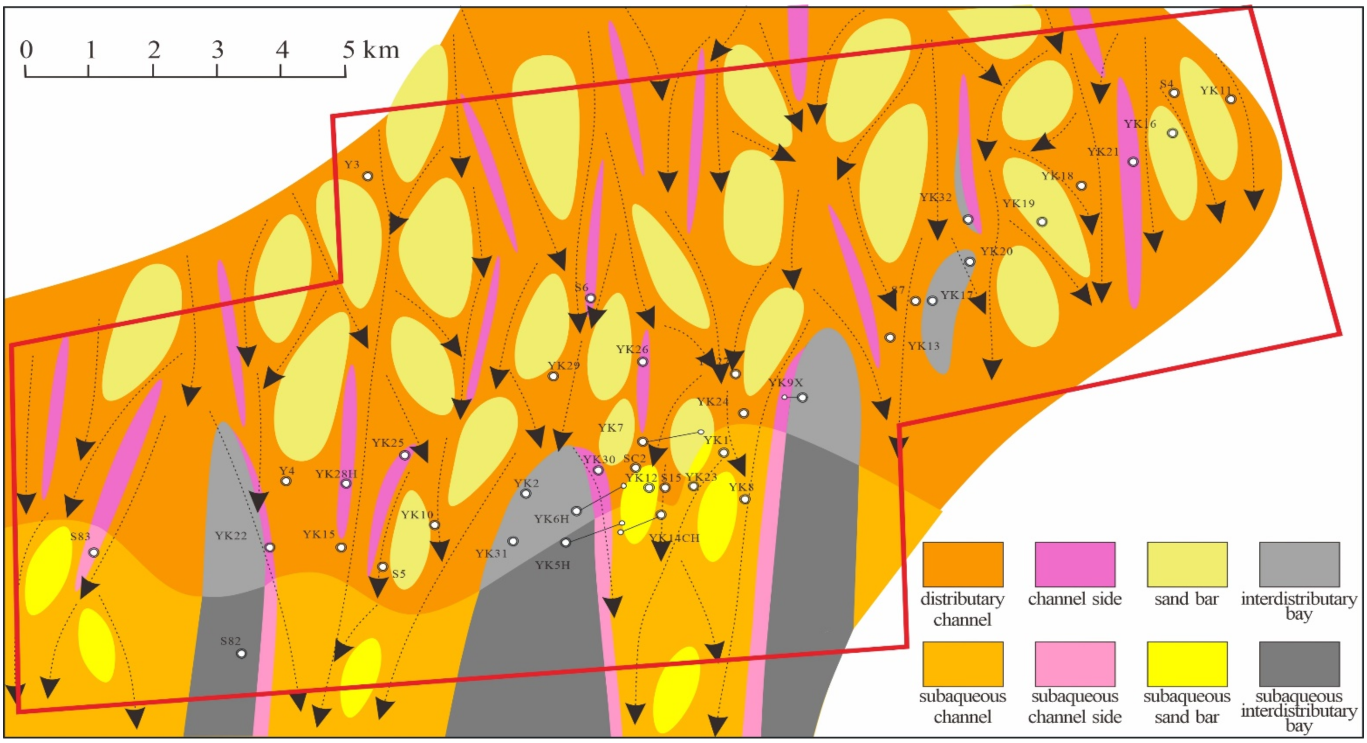

Figure 12. The facies map of a typical layer.

5. Discussion

5.1. Validation of Sandstone Architecture Probability Simulation

New seismic data on the study area had been acquired one year after our work. Since the total thickness of K_1y ranges 28~47 m, which is within or slightly thicker than a seismic wavelength, we still cannot get the fine description of reservoir distribution from the seismic interpretation. We tried to build the facies model through the comprehensive analysis of the amplitude, stacking velocity and other attributes, and adopted geobody interpretation, but it is not possible to specify the attributes to the meter-scale layers. We can check the area ranges of sandbodies and compare them with our simulated ones. We can see from the comparison of the model-extracted facies map and our simulated reservoir distribution map that our simulation results show a reasonable area coverage of sandbars comparing with the facies model (Figure 13).

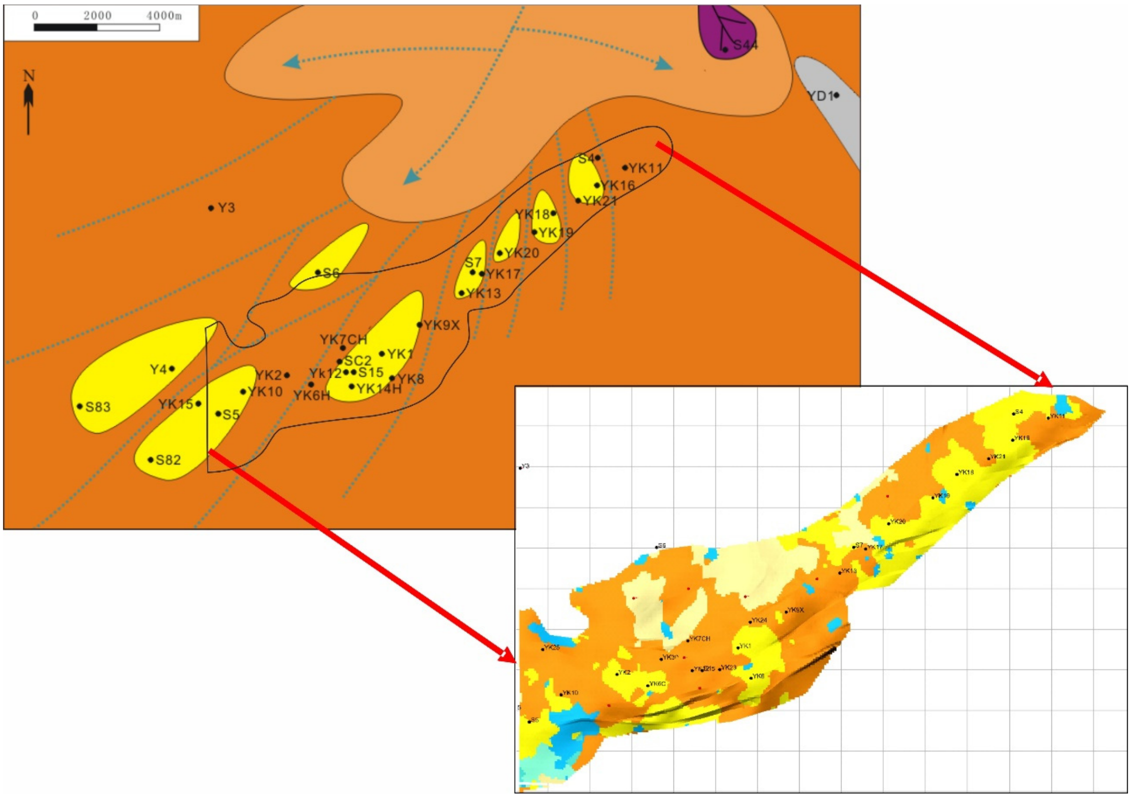

Figure 13. Comparison between the probability simulation results and the petrophysics determined facies model of the upper member of K_1y in Yakela area.

5.2. Applicability of Reservoir Distribution Probability Simulation

As Miall commented in 2006 [6], a continuing effort to develop numerical simulation as the basis for reservoir engineering models is present. Common data on oilfields, such as cores and well logs, are the most direct data we can get for underground, but they are not enough for constraining reservoir models, especially the lateral extension of the reservoir. Hence, analogue and numerical simulation have long been the approaches for reservoir modeling. With the fast development of computer science and technics, we now are able to use big data and numerous simulation methods. What we need is more data, various detailed data of reservoir type, lithology, microfacies and their dimensions, etc. Our work is one effort towards big data and random simulation, and the result has been approved to some extent. We examine this approach to be the most appropriate method, at present, for reservoir distribution estimation in large well-spacing oilfields without proper seismic data.

5.3. Limitation of Probability Simulation

The limitations of our work include: (1) The study area is small, and the sedimentary circle is mid-term to ultrashort term, thus the application of this method to bigger environments needs further validation; (2) We have simulated the connection relationships between different architectural elements, whereas the specific or detailed connection patterns are not as delicate. It is our hope that we can visit more outcrops and obtain more high-resolution seismic profiles to enlarge our reservoir architecture database, then with the help of big data and random simulation, we can be more confident in reservoir architecture analysis and modeling.

6. Conclusions

Architectural elements and their contact relationships in a sandstone reservoir can be determined by core, well logs, and seismic profiles in the areas with sufficient well logging and high-resolution seismic data. However, for the widely spaced well areas without adequate seismic data, the study of reservoir architecture remains difficult. We have made progress in the area of Yakela using Monte Carlo simulation. The major conclusions include:

(1) Well data in Yakela area provides the basic parameters of architectural elements and their contact relationships, based on which we obtained the statistical frequency of vertical developments of sandbodies and then used them as a testing dataset (variables) in the simulation of sandbody architecture.
(2) We measured the sandbody dimensions of a modern sandbar, a similar reservoir, and outcrops and formed a comprehensive database. This database serves as a training dataset in the simulation of sandbody architecture.
(3) We simulated the horizontal development probability of sandbodies in Yakela area from the testing dataset and built the reservoir model to locate favorable reservoir targets. This model fits well with the later seismic interpreted reservoir distribution, suggesting that our simulation is efficient and reliable.
(4) It is of great significance to build a reservoir database with detailed dimensions and parameters of reservoir architectural elements (specific sandbodies). The larger the database is, the more powerfully those new technologies such as big data and deep learning can perform.

Author Contributions: Conceptualization, L.P. and X.W.; methodology, S.C. and T.D.; formal analysis, S.C. and X.W.; resources, H.L.; writing, S.C. and X.W.; project administration, L.P. All authors have read and agreed to the published version of the manuscript.

Funding: This research received no external funding.

Data Availability Statement: Not applicable.

Conflicts of Interest: The authors declare no conflict of interest.

References

1. Pittman, E.D. Porosity, diagenesis and productive capability of sandstone reservoirs. In *Aspects of Diagenesis*; Schoue, P.A., Schluger, P.R., Eds.; SEPM Special Publication: Tulsa, OK, USA, 1979; Volume 26, pp. 159–173.
2. Galloway, W.E. Reservoir facies architecture of microtidal barrier systems. *AAPG Bull.* **1986**, *70*, 787–808.
3. Liu, K.; Boult, P.; Painter, S.; Paterson, L. Outcrop analog for sandy braided stream reservoirs: Permeability patterns in the Triassic Hawkesbury Sandstone, Sydney Basin, Australia. *AAPG Bull.* **1996**, *80*, 1850–1865.
4. Karssenberg, D.; Tornqvist, T.E.; Bridge, J.S. Conditioning a process-based model of sedimentary architecture to well data. *J. Sediment. Res.* **2001**, *71*, 868–879. [CrossRef]
5. Miall, A.D. Architecture and sequence stratigraphy of Pleistocene fluvial systems in the Malay Basin, based on seismic time-slice analysis. *AAPG Bull.* **2002**, *86*, 1201–1216.
6. Miall, A.D. Reconstructing the architecture and sequence stratigraphy of the preserved fluvial record as a tool for reservoir development: A reality check. *AAPG Bull.* **2006**, *90*, 989–1002. [CrossRef]
7. Hampson, G.J.; Sixsmith, P.J.; Johnson, H.D. A sedimentological approach to refining reservoir architecture in a mature hydrocarbon province: The Brent Province, UK North Sea. *Mar. Pet. Geol.* **2004**, *21*, 457–484. [CrossRef]
8. Johannessen, P.N.; Nielsen, L.H. Architecture of an upper Jurassic barrier island sandstone reservoir, Danish Central Graben: Implications of a holocene-recent analogue from the Wadden Sea. *Pet. Geol. Conf.* **2010**, *7*, 145–155. [CrossRef]
9. Siddiqui, N.A.; Ramkumar, M.; Rahman, A.H.A. High resolution facies architecture and digital outcrop modeling of the Sandakan formation sandstone reservoir, Borneo: Implications for reservoir characterization and flow simulation. *Geosci. Front.* **2019**, *10*, 957–971. [CrossRef]
10. Galloway, W.E. Sediments and stratigraphic framework of the copper river fan-delta, Alaska. *J. Sediment. Petrol.* **1976**, *46*, 725–737.
11. Miall, A.D. Reservoir heterogeneities in fluvial sandstones—Lessons from outcrop studies. *AAPG Bull.* **1988**, *72*, 682–697.
12. Smith, R.D.A. Reservoir architecture of syn-rift lacustrine turbidite systems, early cretaceous, offshore south Gabon. In *Geological Society Special Publication*; Lambiase, J.J., Ed.; Geological Society Publishing House: Bath, UK, 1995; pp. 197–210.
13. Richards, M.; Bowman, M. Submarine fans and related depositional systems ii: Variability in reservoir architecture and wireline log character. *Mar. Pet. Geol.* **1998**, *15*, 821–839. [CrossRef]

14. Bruhn, C.H.L. Reservoir architecture of deep-lacustrine sandstones from the Early Cretaceous Recôncavo Rift Basin, Brazil. *AAPG Bull.* **1999**, *83*, 1502–1525.
15. Clark, M.S.; Klonsky, L.F.; Tucker, K.E. Geologic study and multiple 3-D surveys give clues to complex reservoir architecture of giant Coalinga oil field, San Joaquin Valley, California. *Lead Edge* **2001**, *20*, 744–751. [CrossRef]
16. Hornung, J.; Aigner, T. Reservoir architecture in a terminal alluvial plain: An outcrop analogue study (upper Triassic, southern Germany) part 1: Sedimentology and petrophysics. *J. Pet. Geol.* **2002**, *25*, 3–30. [CrossRef]
17. Hampson, G.J.; Rodriguez, A.B.; Storms, J.E.A.; Johnson, H.D.; Meyer, C.T. Geomorphology and high-resolution stratigraphy of progradational wave-dominated shoreline deposits: Impact on reservoir-scale facies architecture. In *Recent Advances in Models of Siliciclastic Shallow-Marine Stratigraphy*; Hampson, G.J., Steel, R.J., Burgess, P.M., Dalrymple, R.W., Eds.; SEPM Special Publication: Tulsa, OK, USA, 2008; Volume 90, pp. 117–142.
18. Sixsmith, P.J.; Hampson, G.J.; Gupta, S.; Johnson, H.D.; Fofana, J.F. Facies architecture of a net transgressive sandstone reservoir analog: The Cretaceous Hosta Tongue, New Mexico. *AAPG Bull.* **2008**, *92*, 513–547. [CrossRef]
19. Sech, R.P.; Jackson, M.D.; Hampson, G.J. Three-dimensional modeling of a shoreface-shelf parasequence reservoir analog: Part 1. Surface-based modeling to capture high-resolution facies architecture. *AAPG Bull.* **2009**, *93*, 1155–1181. [CrossRef]
20. Pyles, D.R.; Syvitski, J.P.M.; Slatt, R.M. Defining the concept of stratigraphic grade and applying it to stratal (reservoir) architecture and evolution of the slope-to-basin profile: An outcrop perspective. *Mar. Pet. Geol.* **2011**, *28*, 675–697. [CrossRef]
21. Onyenanu, G.I.; Jacquemyn, C.E.M.M.; Graham, G.H. Geometry, distribution and fill of erosional scours in a heterolithic, distal lower shoreface sandstone reservoir analogue: Grassy Member, Blackhawk Formation, Book Cliffs, Utah, USA. *Sedimentology* **2018**, *65*, 1731–1760. [CrossRef]
22. Mulhern, J.S.; Johnson, C.L.; Martin, J.M. Modern to Ancient Barrier Island Dimensional Comparisons: Implications for Analog Selection and Paleomorphodynamics. *Front. Earth Sci.* **2019**, *7*, 109. [CrossRef]
23. Johnson, C.L.; Graham, S.A. Sedimentology and Reservoir Architecture of a Synrift Lacustrine Delta, Southeastern Mongolia. *J. Sediment. Res.* **2004**, *74*, 770–785. [CrossRef]
24. Ambrose, W.A.; Hentz, T.F.; Bonnaffé, F. Sequence-stratigraphic controls on complex reservoir architecture of highstand fluvial-dominated deltaic and lowstand valley-fill deposits in the Upper Cretaceous (Cenomanian) Woodbine Group, East Texas field: Regional and local perspectives. *AAPG Bull.* **2009**, *93*, 231–269. [CrossRef]
25. Deveugle, P.E.K.; Jackson, M.D.; Hampson, G.J. Characterization of stratigraphic architecture and its impact on fluid flow in a fluvial-dominated deltaic reservoir analog: Upper Cretaceous Ferron Sandstone Member, Utah. *AAPG Bull.* **2011**, *95*, 693–727. [CrossRef]
26. Hu, W. Reservoir features and controlling factors of Yageliemu Formation in Yakela, Tarim Basin, China. *J. Chengdu Univ. Technol. (Sci. Technol. Ed.)* **2011**, *38*, 385–393, (In Chinese with English Abstract).
27. Walther, J. Einleitung in die Geologie als historische Wissenschaft. In *Lithogenesis der Gegenwart*; G. Fischer, Bd.: Jena, Germany, 1894; Volume 3, pp. 535–1055.
28. Middleton, G. Johannes Walther's Law of Correlation of Facies. *Geol. Soc. Am. Bull.* **1973**, *38*, 979–988. [CrossRef]
29. Zeng, L.; Wang, H.; Gong, L.; Liu, M. Impacts of the tectonic stress field on natural gas migration and accumulation: A case study of the Kuqa Depression in the Tarim Basin, China. *Mar. Pet. Geol.* **2010**, *27*, 1616–1627. [CrossRef]
30. Lai, J.; Wang, G.; Chai, Y.; Xin, Y.; Wu, Q.; Zhang, X.; Sun, Y. Deep burial diagenesis and reservoir quality evolution of high-temperature, high-pressure sandstones: Examples from Lower Cretaceous Bashijiqike Formation in Keshen area, Kuqa depression, Tarim basin of China. *AAPG Bull.* **2017**, *101*, 829–862. [CrossRef]
31. Yao, Z.; He, G.; Li, C.F.; Dong, C. Sill geometry and emplacement controlled by a major disconformity in the Tarim Basin, China. *Earth Planet. Sci. Lett.* **2018**, *501*, 37–45. [CrossRef]
32. Wang, T.F.; Jin, Z.; Li, H.; Liu, D.; Cheng, R.; Shi, S.; Wang, J. Processes and causes of Phanerozoic tectonic evolution of the western Tarim Basin, northwest China. *Pet. Sci.* **2020**, *17*, 279–291. [CrossRef]
33. Liang, L.; Gao, Y.; Zhang, H.; Shao, G.; Yin, T.; Ding, H. Sedimentary Microfacies Analyses of Yageliemu Formation of Yakela Condensate Gas Field in Southern Tianshan Area of Tarim Basin. *Xinjiang Geol.* **2013**, *31*, 66–71, (In Chinese with English Abstract).
34. Kroese, D.P.; Taimre, T.; Botev, Z.I. Handbook of Monte Carlo Methods. In *Wiley Series in Probability and Statistics*; John Wiley & Sons: New York, NY, USA, 2011.
35. Murtha, J.A. Monte Carlo simulation: Its status and future. *J. Pet. Technol.* **1997**, *49*, 361–373. [CrossRef]
36. Cortazar, G.; Schwartz, E.S. Monte Carlo evaluation model of an undeveloped oil field. *J. Energy Financ. Dev.* **1998**, *3*, 73–84. [CrossRef]
37. Ungerer, P.; Tavitian, B.; Boutin, A. *Applications of Molecular Simulation in the Oil and Gas Industry: Monte Carlo Methods*; Editions Technip: Houston, TX, USA, 2005.